Highly-resolved satellite remote sensing based land-use change inventory yields weaker surface albedo-induced global cooling

Xiaohu Jian[1], Xiaodong Zhang[1*], Xinrui Liu[1], Kaijie Chen[1], Tao Huang[2], Shu Tao[1], Junfeng Liu[1], Hong Gao[2], Yuan Zhao[2], Ruiyu Zhugu[1], Jianmin Ma[1]

Correspondence to: Xiaodong Zhang (zhangxd2020@pku.edu.cn)

Supplementary Material 1. OSCAR model configuration

We used the compact earth system model OSCAR v2.4 to assess the impact of land use change (LUC) on albedo-induced radiative forcing (ARF) in the globe (Li et al., 2016; Gasser et al., 2018; Fu et al., 2020; Cherubini et al., 2014). OSCAR is a non-linear box model. It is not a spatially resolved model on a gridded map (i.e., it is not a gridded model) but on a fixed country/regional scale covering 114 countries and regions in the globe. In other words, the OSCAR model used in this study is not gridded but country and regional-based. The OSCAR is a parametric model, in which a relatively large number of parameters required to calculate RF are calibrated on (or input from) complex climate models. Hence, OSCAR performs in a meta-modeling approach. That is, each module of OSCAR is designed to emulate the behavior of other more specialized models (e.g., global climate models, dynamical vegetation models, or chemistry-transport models) (Gasser et al., 2018). Compared with other complex earth system models, the OSCAR has several advantages, including: (1) coupled components: the model has the ability to couple different components of the Earth system, such as the atmosphere and oceans, allowing for the study of complex interactions and feedbacks between these components. (2) The OSCAR ESM is designed in a modular fashion, which means that individual components can be updated or replaced without affecting the entire model. This flexibility makes it easier to incorporate new developments and improve the model over time. (3) The OSCAR can generate Monte Carlo ensembles, which are multiple simulations that vary input parameters randomly. These ensembles can be used to analyze uncertainty and variability, providing statistical analysis of possible outcomes and probabilities. (4) The OSCAR is a simple and compact earth system model. It is designated to diagnose the climate forcing from different climate forcers from their "past" changes rather than future. This enables it to be much easily performed and implemented with the focus on assess quantitatively the

radiative forcing from different climate forcers. These advantages motivate us to choose this tool in our investigations.

Given the fixed national/regional scale in OSCAR, we did not attempt to perform model simulations at different spatial resolutions. Instead, we incorporated ('extrapolated') the updated global LUC data on a 5 km×5 km resolution to 144 countries and regions across the world, which features more detailed land-use evolution, into the OSCAR. This LUC inventory captures the most important land use changes occurring since the early 1980s and provides a unique ecosystem to study the impact of their LUC on climate over a relatively short period, rather than from pre-industrial times, which often generates large uncertainties.

In most previous investigations, radiative forcing due to LUC has been estimated using a radiative transfer model in a GCM (General Circulation Model) (Houghton et al., 1995; Betts et al., 2001; Myhre et al., 2003; Andrews et al., 2017). In OSCAR, the RF from LUC is estimated using a simple parameterization of shortwave radiative forcing. It is parameterized by annually averaged albedo at a biome in a certain region, and the regional shortwave radiation and downward flux at the surface (Bright et al., 2013). A detailed description of the OSCAR v2.4 has been provided by Gasser et al (Gasser et al., 2017). The RF by LUC is simulated using the first-order equation of Bright and Kvalevåg (2013), defined as:

$$\text{RF} = -\pi_{\text{trans}} \sum_i \varphi_{\text{rsds}}^i \sum_b \alpha_{\text{alb}}^{i,b} \frac{\Delta A^{i,b}}{A_{\text{Earth}}} \, , \tag{S1}$$

where $\pi_{\text{trans}} = 0.854$ is the global shortwave and upward transmittance, A_{Earth} denotes the surface area of the Earth (Lenton et al., 2009). φ_{rsds}^i is the yearly averaged downward shortwave radiative flux at the surface that alters with time on an annual basis in region i, which is taken from three projects. These are the Global Energy and Water Exchanges (GEWEX, 2010, https://gewex-srb.larc.nasa.gov/) from 1984-2007, the Clouds and Earth's Radiant Energy System (CERES, 2015,

https://ceres.larc.nasa.gov/) from 2000-2014, and the Modern Era Retrospective-Analysis for Research and Applications (MERRA, 2015, https://gmao.gsfc.nasa.gov/reanalysis/MERRA/) from 1979-2014. $\alpha_{alb}^{i,b}$ in Eq. (S1) is the annually-averaged albedo at the biome b in region i, which is calculated by weighting the albedo climatology by Moderate Resolution Imaging Spectroradiometer (MODIS) (MODIS, 2014, https://modis.gsfc.nasa.gov/), European Space Agency's Climate Change Initiative (ESA-CCI, 2015, https://climate.esa.int/en/), and He et al (He et al., 2014). The albedos used in our study is presented in Table S2. $\Delta A^{i,b}$ is the area of a biome b in region i. ΔA of five land use types in the globe and nine regions is calculated by twenty land-use transitions in Table S1.

Supplementary Material 2. Data and model setup

Fig. S1 and Table S3 compares annual variation of the area of each land use type from 1983 to 2010 between previously used OSCAR LUH1-LUC and GLASS-GLC inventories, including cropland, desert, forest, grassland, and shrubs. Significant differences between the two LUC inventories can be discerned in Fig. S1. As shown, the area change in GLASS-GLC inventory differs by an order of magnitude from the OSCAR LUH1-LUC results, of which, the change in global cropland differs by almost 700 times. The OSCAR LUH1-LUC inventory utilizes a GLM extension model and only combines with satellite-derived current land cover from the Discoverer version 2 (https://heasarc.gsfc.nasa.gov/docs/heasarc/missions/discoverer.html) data using the International Geosphere-Biosphere Programme (IGBP, www.igbp.net) classification map in satellite remote sensing. Whereas, the GLASS-GLC inventory was developed by building the first record of 34-year-long annual dynamics of global land cover (GLASS-GLC) at 5 km×5 km resolution using the Google Earth Engine (GEE)

platform, with the latest version of GLASS (Global Land Surface Satellite) CDRs (climate data records) from 1982 to 2015. GLASS-GLC is characterized by high consistency, more detail, and longer temporal coverage (Liu et al., 2020), thereby yielding more accurate land-use change in the globe.

Since LUH1 dataset does not explicitly categorize urban land cover change and OSCAR v2.4 merely uses LUC data at a coarse spatiotemporal resolution (Hurtt et al., 2011), which would cause large uncertainties in the estimate of albedo-induced RF. To overcome this difficulty, we replaced the OSCAR LUH1-LUC data with updated GLASS-GLC dataset, obtained from Key Laboratory for Earth System Modeling, Department of Earth System Science, Tsinghua University (https://doi.org/10.1594/PANGAEA.913496). This recently updated LUC inventory considers seven major types of land cover in the globe on an annual basis from 1982-2015 and spatial spacing of 5 km×5 km, including cropland, forest, grassland, shrubland, tundra, barren land, and snow/ice. The present assessment focused on five major LU types contributing more significantly to RF. These are cropland, desert, forest, grassland, and shrubs. The same dataset has been used and examined in other studies, demonstrating 82.81% overall accuracy based on 2431 test sample units (Liu et al., 2020).

To distinguish the differences of albedo-induced RF (ARF) between two LUC inventories, we set up two model scenarios in sensitivity experiments by performing OSCAR simulations with low spatiotemporally resolved OSCAR LUH1-LUC inventory (scenario 1) and high spatiotemporally resolved GLASS-GLC inventory (scenario 2), respectively. We also designed 20 sensitivity experiments to reduce respectively by 20% area of LU conversions of each LU type among five LU types from 1982-2010 (Table S1). We estimated disturbance capacity (DC) and effective area (EA) to assess the impact of LUC on the changes in global ARF.

To examine the response of ARF to the spatial resolution of a LUC inventory, we also carried out sensitivity analysis by running the OSCAR model to calculate ARF from 2001 to 2010 using GLASS-GLC inventory on different spatial scales, including 5 km×5 km, 10 km×10 km, 20 km×20 km resolution, and LUH1-LUC on 0.5° × 0.5° latitude/longitude resolution, of which, the 10 km×10 km and 20 km×20 km resolution LUC data was extrapolated from GLASS-GLC inventory on the 5 km×5 km resolution. We estimated the ARF fractions of three GLASS-GLC datasets from 5 km×5 km to 20 km×20 km spacing to the coarse resolution LUH1-LUC inventory. The mean fractions averaged over 2001 to 2010 between the three GLASS-GLC and LUH1-LUC datasets are -16.9%, -14.3%, and -14.1% for the 5 km×5 km, 10 km×10 km, 20 km×20 km resolution GLASS-GLC inventories. As expected, the ARF driven coarse resolution (20 km×20 km) GLASS-GLC differ insignificantly from the 10 km×10 km resolution GLASS-LUC because both datasets are extrapolated from the 5 km×5 km GLASS-GLC. The result suggests that the data sources and approaches to derive a LUC inventory together with spatial resolution determine, to a large extent, the ARF estimation.

Supplementary Material 3. Disturbance capacity and effective area

To explore the global and nine regional inter-annual ARF fluctuations from 1983-2010, we used DC and EA to establish a statistical approach that combines the RF results from 20 sensitivity experiments and the LUC of each target region, as defined in METHOD of main text. A positive DC is associated with a decrease in surface albedo subject to LU conversion and an increase in RF, exerting a warming effect, and vice versa. Here we only discussed the LU conversion subject to those positive DCs. We also calculated the DC of the net LU conversions, which accounts for the two-way conversion of LU types (main text). Results are presented in Table S9 and Table S10.

For instance, the DC for the net LU conversion between grassland and cropland is estimated by the area converted from grassland to cropland minus the area converted from cropland to grassland. Once the DC is obtained, the EA area can be estimated, which defines the converting areas of the 10 net land conversion types between 1982 and 2010 divided by their respective absolute DCs. The results explain the change in ARF from 1983 to 2010.

Globally, net LU conversions with a high DC ($|DC|>1\%$) occurred in grassland to forest, shrub to forest, grassland to cropland, cropland to forest, shrub to cropland, and desert to cropland. Their respective DC values are 19.81%, 12.92%, 6.43%, 5.59%, 3.89%, and 1.33%. The result indicates that the conversion between grassland and forest (DC = 19.81%) exerts the greatest impact on the global ARF. In East and Southeast Asia, the net LU conversion types with large DC values ($|DC|>1\%$) include grassland to forest, shrub to forest, grassland to cropland, cropland to forest, shrub to cropland. Their respective DC values are 13.69%, 5.09%, 13.91%, 15.24% and 1.66%, indicating that the conversion between cropland and forest (DC = 13.69%) plays most significant role in the altered ARF in East and Southeast Asia. In Latin America, the net LU conversions with large DC values ($|DC|>1\%$) occurred in grassland to forest, shrub to forest, grassland to cropland, cropland to forest. Their respective DC values are 38.52%, 7.22%, 2.76%, 1.26%. As a result, the LU conversion between grassland and forest (DC = 38.52%) exert the greatest impact on the changes in ARF in Latin America. In Near East and North Africa, the net LU conversions with large DC values ($|DC|>1\%$) occurred in grassland to forest, shrub to forest, grassland to cropland, cropland to forest, shrub to cropland, and desert to cropland conversion, which are 8.23%, 2.42%, 24.08%, 2.68%, 1.46%, and 11.10%, respectively. Of these LU conversions, the grassland and cropland conversion (DC = 24.08%) contributed the most to the change in ARF in this region. In North America, grassland to forest, grassland to cropland, and cropland to forest conversion were major LU conversion types, which are 34.19%, -8.46%, and

6.84%, respectively, so grassland to forestland conversion dominated ARF variation in this continent. In Sub-Saharan Africa, LU net conversions featured by |DC|>1% occurred in grassland to forest, shrub to forest, grassland to cropland, cropland to forest, and shrub to cropland conversions. Their respective DC values are 13.49%, 24.44%, 2.28%, 1.97%, and 7.80%. In this region, shrub and forest conversion (DC = 24.44%) exerts the greatest impact on the ARF. In South Asia, the net LU conversions with |DC|>1% occurred in grassland to forest, shrub to forest, grassland to cropland, cropland to forest, shrub to cropland, and desert to cropland conversion with their respective DC values at 6.35%, 2.93%, 19.74%, 13.19%, 2.00% and 5.75%. It is straightforward to identify that grassland and cropland conversion (DC = 19.74%) is the most important contributor to the regional ARF in the region. The DCs by net LU conversions in other regions are presented in Table S9.

Supplementary Material 4. Analysis of differences between results of simulations in S1 and S2.

The major reason was significant differences between the GLASS-GLC and original OSCAR LUC inventories (LUH1-LUC). The updated GLASS-GLC includes high-resolution LUC and detailed LU transformation (conversion) between cropland, desert, forest, grassland, and shrubs. Whereas, the LUH1-LUC inventory only considers the one-way inter-conversions between cropland and other four land types.

On the other hand, we can also analyze the reasons from the LUC perspective. The global results are shown in Figure 1. The reason is that in the GLASS-GLC inventory accounts for the global cumulative area of grassland-to-forest conversion from 1982-2010 at 78.67 Mha, the cumulative area of grassland-to-cropland conversion is 90.21 Mha, and the cumulative area of cropland-to-forest conversion at 107.52 Mha, which caused decreasing albedo, and thus ARF_{S2} grown significantly. The LUH1-LUC only

identified a shift of 34.17 Mha from forest to cropland, 25.27 Mha from grassland to cropland, and 12.54 Mha from desert to cropland from 1982 to 2010. Combining these LUC conversion resulted in a smooth increase in ARF_{S1}.

The nine regional results are shown in Figure 2. In East and Southeast Asia, the GLASS-GLC inventory accounts for the cumulative area of grassland-to-forest conversion from 1982-2010 at 15.39 Mha, the cumulative area of grassland-to-cropland conversion is 10.10 Mha, and the cumulative area of cropland-to-forest conversion at 60.51 Mha, which caused decreasing albedo, and thus ARF_{S2} in this region grown significantly. The LUH1-LUC only identified a shift of 29.66 Mha from forest to cropland, 5.40 Mha from grassland to cropland, and 5.25 Mha from desert to cropland from 1982 to 2010. Albedo changes are mainly dominated by the process of conversion of forest to cropland, leading to an increase, and thus ARF_{S1} in this region decreased smoothly.

In Europe, the GLASS-GLC inventory accounts for the cumulative area of grassland-to-forest conversion from 1982-2010 at 4.87 Mha, the cumulative area of desert-to-cropland conversion is 4.73 Mha, and the cumulative area of cropland-to-forest conversion at 4.15 Mha, which caused decreasing albedo, and thus ARF_{S2} in this region grown significantly. The LUH1-LUC only identified a shift of 10.73 Mha from forest to cropland, 4.42 Mha from grassland to cropland, and 3.02 Mha from desert to cropland from 1982 to 2010. Combining these LUC conversion resulted in a smooth increase of ARF_{S1} in this region. In Latin America, the GLASS-GLC inventory accounts for the cumulative area of forest-to-grassland conversion from 1982-2010 at 41.10 Mha, and the cumulative area of cropland-to-forest conversion at 4.34 Mha, which caused increasing albedo, and thus ARF_{S2} in this region decreased significantly. The LUH1-LUC only identified a shift of 18.60 Mha from forest to cropland, 2.76 Mha from shrub to cropland, and 2.93 Mha from desert to cropland from 1982 to 2010. Combining these LUC conversion resulted in a significant decrease of ARF_{S1} in this region.

In Near East and North Africa, the GLASS-GLC inventory accounts for the cumulative area of grassland-to-forest conversion from 1982-2010 at 1.30 Mha, the cumulative area of grassland-to-cropland conversion is 6.57 Mha, and the cumulative area of cropland-to-forest conversion at 3.72 Mha, which caused decreasing albedo, and thus ARF_{S2} in this region grown significantly. The LUH1-LUC only identified a process of increasing (2.43Mha from 1982-1995) and then decreasing (-1.35Mha from 1995-2010) cropland area, resulting in a slow increase and then a slow decrease in ARF_{S1} in this region.

In North America, the GLASS-GLC inventory accounts for the cumulative area of grassland-to-forest conversion from 1982-2010 at 27.13 Mha, the cumulative area of grassland-to-cropland conversion is 17.47 Mha, and the cumulative area of cropland-to-forest conversion at 11.59 Mha, which caused decreasing albedo, and thus ARF_{S2} in this region grown significantly. The LUH1-LUC only identified a shift of 14.10 Mha from cropland to forest, 5.73 Mha from cropland to grassland, and 2.59 Mha from cropland to desert from 1982 to 2010. Combining these LUC conversion resulted in a smooth increase of ARF_{S1} in this region.

In Oceania, the GLASS-GLC inventory accounts for the cumulative area of grassland-to-forest conversion from 1982-2010 at 2.63 Mha, the cumulative area of shrub-to-forest conversion is 1.61 Mha, and the cumulative area of cropland-to-forest conversion at 0.97 Mha, which caused decreasing albedo, and thus ARF_{S2} in this region grown significantly. The LUH1-LUC only identified a shift of 1.39 Mha from cropland to forest, 1.58 Mha from cropland to grassland (In Oceania, albedo is higher in cropland than in grassland, as shown in Table S2), and 0.48 Mha from cropland to shrub from 1982 to 2010. Combining these LUC conversion resulted in a significant increase of ARF_{S1} in this region.

In Russia, the GLASS-GLC inventory accounts for the cumulative area of grassland-to-forest conversion from 1982-2010 at 53.10 Mha, and the cumulative area

of cropland-to-grassland conversion at 3.37 Mha (In Russia, albedo is higher in cropland than in grassland, as shown in Table S2), which caused decreasing albedo, and thus ARF_{S2} in this region grown significantly. The LUH1-LUC only identified a shift of 5.59 Mha from cropland to forest, 3.13 Mha from cropland to grassland, and 0.60 Mha from cropland to shrub from 1982 to 2010. Combining these LUC conversion resulted in a smooth increase of ARF_{S1} in this region.

In Sub-Saharan Africa, the GLASS-GLC inventory accounts for the cumulative area of grassland-to-forest conversion from 1982-1993 at 73.82 Mha, the cumulative area of shrub-to-forest conversion at 35.13 Mha, and the cumulative area of cropland-to-forest conversion at 10.46 Mha, which caused decreasing albedo, and thus ARF_{S2} grown significantly. In 1993-2010, the GLASS-GLC inventory accounts for the cumulative area of forest-to-grassland conversion at 61.46 Mha, the cumulative area of forest-to-shrub conversion at 76.19 Mha, and the cumulative area of cropland-to-forest conversion at 3.74 Mha, which caused increasing albedo, and thus ARF_{S2} decreased significantly. The LUH1-LUC only identified a shift of 22.26 Mha from grassland to cropland, 17.84 Mha from cropland to forest, and 9.11 Mha from desert to cropland from 1982 to 2010. Combining these LUC conversion resulted in a smooth increase of ARF_{S1} in this region.

In South Asia, the GLASS-GLC inventory accounts for the cumulative area of grassland-to-forest conversion from 1982-2010 at 2.99 Mha, the cumulative area of cropland-to-forest 16.37 Mha, and the cumulative area of grassland-to-cropland conversion at 24.75 Mha, which caused decreasing albedo, and thus ARF_{S2} in this region grown significantly. The LUH1-LUC only identified a shift of 2.25 Mha from desert to cropland, 0.39 Mha from cropland to forest, and 1.20 Mha from grassland to cropland from 1982 to 2010. Combining these LUC conversion resulted in a smooth increase of ARF_{S1} in this region.

Supplementary Material 5. Sensitivity experiments

We designed 20 sensitivity experiments among five land use types (cropland, desert, forest, grassland, and shrub) to explore potential causes of RF fluctuations in the globe and nine regions from 1983 to 2010. In each experiment, we reduced the LU transition area by 20% in year t as presented in Table S1. We used DC and EA to interpret the results from the 20 sensitivity experiments (MHTHODS, Text S3). We selected the annual LU conversion areas subject to six LU transformation types having most prominent impact on global ARF based on the magnitude of |DC|>1%. The results are also compared to their respective contribution to the altered ARF, defined as ARF_d and calculated by

$$ARF_{di}^t = (RF^t - RF^{t-1}) - (RF_i'^{\ t} - RF_i'^{\ t-1}),$$

where RF^t and $RF_i'^{\ t}$ are changes in global ARF ARF from sensitivity experiments for LU conversion type i in year t. We choose ARF_d>0.01 m W m^{-2} to characterize the rate and extent of changes in ARF subject to LU transitions. Based on the results of Table S7 and Fig. S15, we select six LU transformation types in the globe, including grassland to forest, shrub to forest, grassland to cropland, cropland to forest, shrub to cropland, and desert to cropland.

The ARF_d in the selected LU conversion types under the same selection criteria (|DC|>1% and ARF_d>0.01 m W m^{-2}) for each of nine regions and the globe are illustrated in Figs. S3-S12.

Supplementary Material 6. Further readings in Figure 3

Here we further analyze the relationships between RF and EAs in other regions, which are not discussed in main text. In Europe, the correlation coefficient (rr) between ARF and the EA is 0.860 (P-value<0.01). In this case the EA consists of a cumulative

area of four net LU conversion types, namely grassland to forest, grassland to cropland, cropland to forest, and desert to cropland, accounting for 46.00%, 37.70%, 12.60%, and 3.60% in the total EA, respectively. In Near East and North Africa, *rr* between ARF and the effective area is 0.934 (*P*-value<0.01) and the EA includes a cumulative area of six net LU conversion types, namely grassland to forest, shrub to forest, grassland to cropland, cropland to forest, shrub to cropland and desert to cropland, contributing 16.50%, 4.90%, 48.20%, 5.40%, 2.90%, and 22.20% to the total effective area in this region, respectively. In North America, *rr* between ARF and the EA is 0.867 (*P*-value<0.01), which includes the cumulative area of three net LU conversion types. These are grassland to forest, grassland to crop, and cropland to forest, accounting for 69.10%, -17.10%, and 13.80% of the total effective area in this continent, respectively. In Oceania, *rr* between ARF and the EA is 0.531 (*P*-value<0.01), the latter consists of a cumulative area with five net LU conversion types, including grassland to forest, shrub to forest, grassland to cropland, cropland to forest, and shrub to cropland, accounting for 34.70%, 44.00%, -9.00%, 7.70%, and -4.60% of the total effective area in Oceania, respectively. In Russia, strong correlation coefficient of 0.953 (*P*-value<0.01) between ARF and effective area was observed. In this case, the EA includes a cumulative area of three net LU conversion types. These are grassland to forest, grassland to crop, and cropland to forest, contributing 78.00%, -17.60%, and 4.40% to the total effective area in Russia, respectively.

Supplementary Material 7. ARF from forest, grassland, and shrubland transition

As can be seen in Fig. 5a-c, the ARF from fixed forestland is, in general, lower than the ARF from scenario 2 result because in most years of 1983 through 2010, the ARFs from scenario 2 with fixed LUC (blue solid line) is below the ARF derived from altered LUC under scenario 2 (red solid line). We observe a mean percentage-change

in ARF over 5% between fixed and altered forestland in scenario 2 averaged from 1983-2010. The annual percentage change reaches a maximum of 32% in 2009 (Table S1). The bar charts in the inset of Fig. 5a-c show that the conversions from cropland and grassland to forestland contribute 52.11% and 38.13% to the change in forestland between 1983 and 2010, respectively. Rather, desert-to-forest conversion and shrub-to-forest conversion merely contribute 0.52% and -9.24% to the change in forestland for the same period. Since the conversions from cropland and grassland to forestland under scenario 2 reduces the surface albedo, which, in turn, reduces a negative ARF. On the other hand, due to lower surface albedo on forestland, the fixed forestland yields greater negative ARF values, as seen in Fig. 5a-c. The result manifests that the cropland and grassland to forestland transitions weakens the cooling effect. Likewise, smaller negative ARF values from the transitions between cropland (Fig. 5a-a) and grassland (Fig. 5a-d) and the other four LU types are also identified. From the inset bar chart figure of Fig. 5a-a, we can discern that the transitions from cropland to forestland (negative bar) and grassland and desert to cropland (positive bar) dominate the LU conversions. The net transition yields smaller negative ARF values and hence weaker cooling effect compared to the ARF from fixed cropland with significantly lower albedo than grassland and desert (Table S2). This result is also applicable in the altered ARF driven by transitions between grassland and the other four LU types (Fig. 5a-d), in which the transitions from grassland to shrubland (-28.32%), grassland to forestland (-16.17%) and cropland (-18.54%) overwhelm desert to grassland (36.97%) transition (the inset bar chart of Fig. 5a-d), yielding a net conversion area of -26.06%, suggesting that the reduction of grassland results in smaller negative ARF values and reducing the cooling effect compared to ARF from the fixed grassland.

In contrast, in the case of LU transition between shrubland and the other four LU types, the transition from grassland (74.52%), forestland (10.31%), and desert (14.11%) to shrubland dominates the LUC. As a result, global shrublands expanded at a mean

14

growth rate of 6.6 Mha/yr (Fig. S14e), which yields larger negative ARF values compared to the fixed shrubland because of overall reduced albedo from such LU transition in the globe (Table S2).

Table S1. Twenty OSCAR sensitivity experiments considering conversions among five major land-use types in GLASS-GLC dataset

Sensitivity experiment	Land Use Type	Conversion
1	Crop	crop to desert
2	-	crop to forest
3	-	crop to grass
4	-	crop to shrub
5	Desert	desert to crop
6	-	desert to forest
7	-	desert to grass
8	-	desert to shrub
9	Forest	forest to crop
10	-	forest to desert
11	-	forest to grass
12	-	forest to shrub
13	Grass	grass to crop
14	-	grass to desert
15	-	grass to forest
16	-	grass to shrub
17	Shrub	shrub to crop
18	-	shrub to desert
19	-	shrub to forest
20	-	shrub to grass

Table S2. Albedo in each country/region over the five land use types in OSCAR (Gasser, 2017) and regrouped nine regions in the globe.

Region	Number	Country/region	Albedo				
-			Cropland	Desert	Forest	Grassland	Shrubland
	1	China	0.188	0.269	0.141	0.230	0.148

East and Southeast Asia	2	Japan	0.146	0.139	0.160	0.160	0.160
	3	Korea	0.148	0.133	0.136	0.136	0.136
	4	Taiwan	0.153	0.145	0.128	0.151	0.132
	5	Cambodia	0.172	0.153	0.146	0.151	0.152
	6	Rest of East Asia	0.247	0.278	0.168	0.280	0.221
	7	Hong Kong	-	-	-	-	-
	8	Indonesia	0.163	0.143	0.146	0.163	0.156
	9	Lao People's Democratic Republic	0.165	0.150	0.144	0.150	0.149
	10	Myanmar	0.172	0.147	0.137	0.143	0.146
	11	Malaysia	0.168	0.119	0.149	0.167	0.157
	12	Philippines	0.164	0.156	0.153	0.162	0.159
	13	Singapore	0.165	0.109	0.165	0.162	0.163
	14	Thailand	0.175	0.154	0.145	0.155	0.152
	15	Vietnam	0.167	0.146	0.141	0.149	0.146
	16	Rest of Southeast Asia	0.157	0.156	0.150	0.157	0.152
	1	Austria	0.179	0.209	0.165	0.186	0.164
	2	Belgium	0.180	0.170	0.169	0.169	0.168
	3	Czech Republic	0.178	0.168	0.164	0.165	0.163
	4	Denmark	0.185	0.160	0.177	0.174	0.179
	5	Estonia	0.181	0.160	0.165	0.166	0.166
	6	Finland	0.168	0.167	0.169	0.175	0.171
	7	France	0.180	0.204	0.155	0.178	0.145
	8	Germany	0.180	0.187	0.163	0.177	0.164
	9	Greece	0.165	0.129	0.131	0.132	0.126
	10	Hungary	0.177	0.180	0.178	0.178	0.179
	11	Ireland	0.198	0.199	0.169	0.196	0.161
	12	Italy	0.164	0.271	0.167	0.207	0.156
	13	Latvia	0.193	0.172	0.173	0.174	0.174
	14	Lithuania	0.194	0.165	0.180	0.182	0.182
	15	Luxembourg	0.162	0.166	0.159	0.165	0.160
	16	Malta	-	-	-	-	-

Europe	17	Netherlands	0.169	0.186	0.146	0.184	0.154
	18	Poland	0.184	0.176	0.164	0.169	0.168
	19	Portugal	0.160	0.135	0.126	0.130	0.137
	20	Slovakia	0.178	0.171	0.164	0.165	0.164
	21	Slovenia	0.174	0.154	0.153	0.157	0.157
	22	Spain	0.183	0.184	0.150	0.152	0.154
	23	Sweden	0.167	0.196	0.150	0.164	0.154
	24	United Kingdom	0.181	0.202	0.199	0.200	0.210
	25	Switzerland	0.162	0.266	0.187	0.213	0.186
	26	Norway	0.163	0.316	0.173	0.231	0.195
	27	Rest of EFTA	0.300	0.252	0.274	0.216	0.249
	28	Albania	0.166	0.164	0.172	0.165	0.160
	29	Bulgaria	0.177	0.159	0.161	0.160	0.161
	30	Belarus	0.194	0.201	0.176	0.182	0.176
	31	Croatia	0.171	0.152	0.159	0.158	0.158
	32	Romania	0.183	0.183	0.167	0.174	0.167
	33	Ukraine	0.185	0.160	0.168	0.168	0.168
	34	Rest of Eastern Europe	0.175	0.150	0.172	0.142	0.150
	35	Rest of Europe	0.177	0.180	0.172	0.173	0.170
	36	Rest of Former Soviet Union	0.223	0.257	0.249	0.272	0.241
Latin America	1	Mexico	0.160	0.184	0.140	0.155	0.181
	2	Argentina	0.176	0.175	0.134	0.148	0.145
	3	Bolivia	0.173	0.197	0.144	0.146	0.137
	4	Brazil	0.166	0.163	0.146	0.154	0.156
	5	Chile	0.143	0.273	0.129	0.154	0.163
	6	Colombia	0.181	0.166	0.147	0.165	0.154
	7	Ecuador	0.164	0.061	0.146	0.145	0.146
	8	Paraguay	0.166	0.153	0.142	0.148	0.146
	9	Peru	0.166	0.188	0.145	0.156	0.143
	10	Uruguay	0.181	0.182	0.166	0.181	0.170
	11	Venezuela	0.179	0.168	0.144	0.168	0.146

	12	Rest of South America	0.167	0.165	0.145	0.162	0.160
	13	Costa Rica	0.171	0.147	0.158	0.166	0.164
	14	Guatemala	0.158	0.156	0.151	0.146	0.149
	15	Nicaragua	0.172	0.155	0.169	0.156	0.176
	16	Panama	0.173	0.174	0.161	0.173	0.168
	17	Rest of Central America	0.155	0.148	0.153	0.148	0.149
	18	Caribbean	0.170	0.105	0.151	0.158	0.155
Near East and North Africa	1	Cyprus	0.171	0.185	0.131	0.147	0.151
	2	Kazakhstan	0.264	0.245	0.218	0.250	0.241
	3	Kyrgyzstan	0.242	0.288	0.272	0.289	0.294
	4	Armenia	0.235	0.234	0.180	0.245	0.215
	5	Azerbaijan	0.178	0.176	0.184	0.210	0.181
	6	Georgia	0.233	0.236	0.186	0.208	0.172
	7	Turkey	0.206	0.251	0.158	0.203	0.162
	8	Rest of Western Asia	0.192	0.303	0.213	0.160	0.145
	9	Egypt	0.190	0.358	0.161	0.160	0.159
	10	Morocco	0.182	0.250	0.155	0.169	0.171
	11	Tunisia	0.196	0.336	0.143	0.214	0.272
	12	Rest of North Africa	0.195	0.369	0.148	0.195	0.190
North America	1	Canada	0.253	0.274	0.166	0.218	0.174
	2	United States of America	0.212	0.200	0.148	0.192	0.200
	3	Rest of North America	-	-	-	-	-
Oceania	1	Australia	0.192	0.194	0.123	0.156	0.150
	2	New Zealand	0.176	0.198	0.120	0.172	0.130
	3	Rest of Oceania	0.157	0.143	0.146	0.153	0.146

Russia	1	Russian Federation	0.233	0.228	0.185	0.212	0.192
Sub-Saharan Africa	1	Nigeria	0.234	0.308	0.163	0.200	0.170
	2	Senegal	0.250	0.284	0.243	0.266	0.190
	3	Rest of Western Africa	0.219	0.384	0.153	0.254	0.165
	4	Rest of Central Africa	0.214	0.378	0.144	0.193	0.154
	5	Rest of South Central Africa	0.151	0.235	0.135	0.142	0.138
	6	Ethiopia	0.150	0.202	0.137	0.150	0.148
	7	Madagascar	0.145	0.167	0.140	0.166	0.149
	8	Malawi	0.153	0.143	0.144	0.142	0.143
	9	Mauritius	-	-	-	-	-
	10	Mozambique	0.153	0.141	0.141	0.143	0.142
	11	Tanzania	0.164	0.160	0.140	0.147	0.146
	12	Uganda	0.157	0.153	0.150	0.151	0.154
	13	Zambia	0.149	0.146	0.124	0.138	0.138
	14	Zimbabwe	0.164	0.152	0.148	0.150	0.148
	15	Rest of Eastern Africa	0.202	0.282	0.149	0.200	0.165
	16	Botswana	0.168	0.211	0.148	0.204	0.160
	17	South Africa	0.162	0.195	0.143	0.181	0.143
	18	Rest of South African Customs Union	0.186	0.210	0.149	0.178	0.141
South	1	Bangladesh	0.157	0.150	0.142	0.152	0.151
	2	India	0.178	0.314	0.138	0.257	0.247
	3	Pakistan	0.195	0.227	0.142	0.221	0.272
	4	Sri Lanka	0.156	0.153	0.152	0.158	0.154

| Asia | 5 | Rest of South Asia | 0.189 | 0.265 | 0.124 | 0.250 | 0.200 |
| | 6 | Iran | 0.210 | 0.223 | 0.153 | 0.221 | 0.207 |

Table S3. Area of land-use change in five land-use types from 1982 to 2010 in each of selected nine regions in OSCAR LUH1-LUC dataset and GLASS-GLC dataset. Negative values indicate declining area of a LU type on an annual basis from 1982 to 2010 and positive values indicate expanding area.

Region	Area (Mha / yr) of OSCAR LUC dataset					Area (Mha / yr) of GLASS-GLC dataset				
-	Cropland	Desert	Forest	Grassland	Shrubland	Cropland	Desert	Forest	Grassland	Shrubland
Global	2.765	-0.448	-1.221	-0.902	-0.194	0.041	-8.865	7.779	-3.411	6.604
East and South-east Asia	1.481	-0.188	-1.059	-0.193	-0.041	-1.514	-0.709	2.866	-0.124	-0.386
Europe	-0.670	0.108	0.383	0.158	0.021	-0.523	-0.316	0.387	0.502	-0.002
Latin America	1.253	-0.105	-0.664	-0.385	-0.099	0.889	-0.243	-0.830	-0.708	0.908
Near East and North Africa	0.039	-0.045	0.018	-0.017	0.005	0.352	-1.417	0.197	0.681	0.173
North America	-0.827	0.092	0.503	0.205	0.026	0.212	-1.201	1.819	-0.476	-0.065
Oceania	-0.161	0.038	0.050	0.056	0.017	0.008	-1.799	0.186	0.050	1.556
Russia	-0.389	0.056	0.199	0.112	0.021	-0.075	-0.453	3.225	-1.125	0.000
Sub-Saharan Africa	1.883	-0.325	-0.637	-0.795	-0.126	0.248	-1.770	-0.785	-2.102	4.407
South Asia	0.156	-0.080	-0.014	-0.043	-0.019	0.444	-0.957	0.713	-0.110	0.013

Table S4. Results of a_{ik} (see 'Method') and significance tests on effective area. a_{ik} means the ratio of different net LU conversion to the global effective area. For example, a_{ik} in the immediate cell below NetGar2for is 0.396, indicating that NetGar2for accounts for 39.6% of global effective area.

	Net Gra2for	Net Shr2for	Net Gra2cro	Net Cro2for	Net Shr2cro	Net Des2cro	Other conversion	R-value	P-value
Global	0.396	0.259	0.129	0.112	0.078	0.027	0.000	0.765	<0.01[**]
East and South-east Asia	0.276	0.103	0.280	0.307	0.033	0.000	0.000	0.930	<0.01[**]
Europe	0.460	0.000	0.377	0.126	0.000	0.036	0.000	0.860	<0.01[**]
Latin America	0.774	0.145	0.055	0.025	0.000	0.000	0.000	0.846	<0.01[**]
Near East and North Africa	0.165	0.049	0.482	0.054	0.029	0.222	0.000	0.934	<0.01[**]
North America	0.691	0.000	-0.171	0.138	0.000	0.000	0.000	0.867	<0.01[**]
Oceania	0.347	0.440	-0.090	0.077	-0.046	0.000	0.000	0.531	<0.01[**]
Russia	0.780	0.000	-0.176	0.044	0.000	0.000	0.000	0.953	<0.01[**]
Sub-Saharan Africa	0.270	0.489	0.046	0.039	0.156	0.000	0.000	0.834	<0.01[**]
South Asia	0.127	0.059	0.395	0.264	0.040	0.115	0.000	0.970	<0.01[**]

Table S5. ARF (W m^{-2}) and ARF trend (W m^{-2} yr^{-1}) over the nine regions between 1983 and 2010 from S1 and S2 scenario modeling. The maximum, minimum, and mean percentage changes (%) and the trend of percentage change (% yr^{-1}) are also presented.

	S1 scenario			S2 scenario			Percentage change			
	1983	2010	Trend	1983	2010	Trend	Max	Min	Mean	Trend
East and South-east Asia	-0.028	-0.031	-7.03×10^{-5}	-0.027	-0.011	5.93 ×10^{-4}	-0.84 in 1993	-70.8 In 2009	-28.48	-2.15
Europe	7.64 ×10^{-3}	7.83 ×10^{-3}	3.00 × 10^{-6}	6.14 ×10^{-3}	8.91 ×10^{-3}	1.93 × 10^{-4}	37.02 in 2008	-64.08 in 1985	-7.15	2.46
Latin America	-0.031	-0.034	-1.34×10^{-4}	-0.029	-0.033	-1.09 × 10^{-4}	-14.32 In 1984	8.91 In 1999	0.18	-0.07

21

Near East and North Africa	9.75×10^{-3}	8.06×10^{-3}	-8.00×10^{-5}	8.17×10^{-3}	1.44×10^{-2}	2.58×10^{-4}	78.64 in 2010	-44.1 in 1989	25.09	3.90
North America	-3.19×10^{-2}	-2.90×10^{-2}	1.03×10^{-4}	-3.51×10^{-2}	-2.70×10^{-2}	3.19×10^{-4}	18.94 in 1999	-17.93 in 2008	5.11	-0.70
Oceania	-3.22×10^{-2}	-2.84×10^{-2}	1.07×10^{-4}	-3.18×10^{-2}	-2.81×10^{-2}	1.05×10^{-4}	1.43 in 1997	-4.62 In 1984	-0.36	3.93×10^{-3}
Russia	-6.75×10^{-3}	-5.89×10^{-3}	3.75×10^{-5}	-9.05×10^{-3}	-2.90×10^{-3}	3.02×10^{-4}	57.63 in 1999	-94.47 in 2008	10.33	-4.18
Sub-Saharan Africa	-0.057	-0.050	2.81×10^{-4}	-0.051	-0.061	-2.61×10^{-4}	53.38 in 1990	-75.72 in 1994	6.78	1.05
South Asia	0.011	0.012	4.16×10^{-5}	0.012	0.020	3.66×10^{-4}	70.21 in 2008	5.44 in 1989	37.30	2.62

Table S6. Contribution (%) of six major net LU transitions to the changes in ARF from 1983 to 2010. The coefficient of variation (CV) is $\pm5\%$.

	Net Gra2for	Net For2shr	Net Gra2cro	Net Cro2for	Net Cro2shr	Net Des2cro
East and South-east Asia	19.50	0.16	7.47	16.71	3.42	0.62
Europe	8.16	-0.01	-9.37	2.40	-1.47	1.97
Latin America	-8.71	3.54	1.05	1.64	5.75	-0.05
Near East and North Africa	4.15	1.01	7.85	3.07	-2.29	9.30
North America	14.22	0.57	-0.51	7.77	5.33	0.16
Oceania	0.44	-0.31	0.85	0.97	5.61	-0.26
Russia	15.74	0.03	0.39	0.26	0.59	-0.07
Sub-Saharan	14.29	-55.49	15.22	4.76	-16.31	-0.50

Africa						
South Asia	2.35	0.35	10.09	6.22	-4.42	1.30
Global	70.14	-50.15	33.04	43.79	-3.80	12.47

Table S7. Contribution (%) of six major net LUCs from 1983 to 2010 to global effective area

	Net Gra2for	Net For2shr	Net Gra2cro	Net Cro2for	Net Cro2shr	Net Des2cro
East and South-east Asia	-1.76	-7.33	1.39	-1.93	-0.75	0.40
Europe	1.87	-0.01	0.04	8.77	-0.02	0.17
Latin America	20.36	-22.66	4.88	-0.22	3.53	0
Near East and North Africa	0.26	0.73	0.89	1.04	0.23	1.11
North America	4.89	1.74	0.51	3.36	0	0
Oceania	1.49	-0.65	0.71	-0.13	0.08	0.47
Russia	6.91	0	1.91	0.72	0	0.10
Sub-Saharan Africa	5.91	54.43	0.35	-1.10	4.34	-0.12
South Asia	-0.33	-0.34	2.21	0.67	0.40	0.57
Global	39.60	25.90	12.90	11.20	7.80	2.70

Table S8. Contribution (%) of five LU types from 1983 to 2010 in nine regions to the changes in global ARF. The coefficient of variation (CV) is $\pm 5\%$.

	Cropland	Desert	Forest	Grassland	Shrub
East and South-east Asia	14.11	-0.08	18.04	13.25	1.55

Europe	-3.24	1.05	5.36	-0.62	-0.75
Latin America	4.19	-0.07	-1.77	-3.86	4.60
Near East and North Africa	8.97	5.26	4.31	6.42	-0.20
North America	6.37	0.41	11.50	6.96	3.05
Oceania	3.59	-0.54	0.39	0.40	2.40
Russia	0.59	-0.04	8.03	8.06	0.30
Sub-Saharan Africa	1.58	-0.66	-18.39	14.47	-36.18
South Asia	6.59	0.60	4.46	6.18	-2.08
Globe	42.76	5.94	31.91	51.26	-27.31

Table S9. Disturbance capacity (%) of 10 net LU conversions in the globe and nine regions by summing two-way LU conversions.

	Global	East and South-east Asia	Europe	Latin America	Near East and North Africa	North America	Oceania	Russia	Sub-Saharan Africa	South Asia
Net Gra2for	19.809	13.686	22.847	38.521	8.226	34.190	17.048	38.923	13.492	6.354
Net Shr2for	12.918	5.092	0.126	7.219	2.423	0.265	21.662	-0.043	24.442	2.928
Net Gra2cro	6.429	13.907	18.749	2.757	24.080	-8.462	-4.423	-8.774	2.275	19.737
Net Cro2for	5.593	15.242	6.282	1.255	2.682	6.837	3.788	2.178	1.968	13.194
Net Shr2cro	3.886	1.660	0.036	0.177	1.455	-0.031	-2.265	0.006	7.798	1.999
Net Des2cro	1.331	0.403	1.812	0.020	11.100	-0.018	-0.712	-0.021	0.018	5.754
Net Des2for	0.035	0.003	0.142	0.025	-0.013	0.185	0.066	0.051	-0.002	-0.012
Net Des2gra	0.000	-0.002	-0.001	0.009	-0.008	-0.002	-0.003	0.003	0.001	-0.011
Net Des2shr	0.000	-0.001	0.001	-0.008	-0.007	0.003	0.013	-0.001	0.002	-0.003
Net Gra2shr	0.000	-0.003	-0.004	0.008	-0.005	0.007	0.018	0.001	0.002	-0.008

Table S10. Disturbance capacity (%) of 20 land conversion types in the globe and nine regions

	Global	East and South-east Asia	Europe	Latin America	Near East and North Africa	North America	Oceania	Russia	Sub-Saharan Africa	South Asia
grass to forest	20.252	14.264	21.876	38.729	7.305	34.169	22.992	38.094	14.596	5.149
forest to grass	-19.366	-13.109	-23.817	-38.313	-9.147	-34.212	-11.103	-39.752	-12.388	-7.560
shrub to forest	12.574	5.156	0.026	7.815	2.233	0.515	22.355	-0.010	23.540	2.604
forest to shrub	-13.261	-5.028	-0.226	-6.623	-2.614	-0.016	-20.970	0.076	-25.344	-3.252
grass to crop	6.606	14.161	18.686	2.874	24.578	-8.510	-4.347	-8.918	2.378	21.033
crop to grass	-6.252	-13.653	-18.812	-2.641	-23.582	8.415	4.499	8.630	-2.172	-18.441
crop to forest	5.763	15.865	6.157	1.381	2.665	6.913	4.007	2.163	2.039	13.912
forest to crop	-5.423	-14.620	-6.408	-1.130	-2.700	-6.762	-3.569	-2.194	-1.898	-12.476
shrub to crop	3.914	1.745	0.033	0.200	1.368	0.044	-2.140	0.001	7.841	1.901
crop to shrub	-3.858	-1.575	-0.038	-0.155	-1.541	0.018	2.391	0.011	-7.755	-2.097
desert to crop	1.383	0.432	1.893	0.017	11.454	-0.007	-0.585	-0.018	0.013	5.969
crop to desert	-1.279	-0.373	-1.732	0.023	-10.746	0.029	0.840	0.025	-0.022	-5.539
desert to forest	0.037	0.006	0.153	0.018	-0.015	0.200	0.096	0.054	-0.003	-0.014
forest to desert	-0.033	-0.001	-0.130	-0.032	-0.012	-0.170	0.036	-0.047	0.002	-0.010
desert to grass	0.000	-0.001	-0.002	0.010	-0.012	0.000	-0.001	0.004	0.001	-0.008
grass to desert	0.000	-0.003	-0.001	0.008	-0.003	-0.003	-0.005	0.002	-0.001	0.014
desert to shrub	0.000	-0.002	0.001	-0.012	-0.005	0.000	0.022	-0.001	0.003	-0.003
shrub to desert	0.000	-0.001	-0.001	-0.005	0.009	-0.005	-0.004	0.001	0.001	0.003
grass to shrub	0.000	-0.003	-0.004	0.004	-0.007	0.007	0.011	0.001	0.001	-0.011
shrub to grass	0.000	-0.004	-0.003	-0.011	-0.004	0.007	0.022	0.001	0.003	-0.004
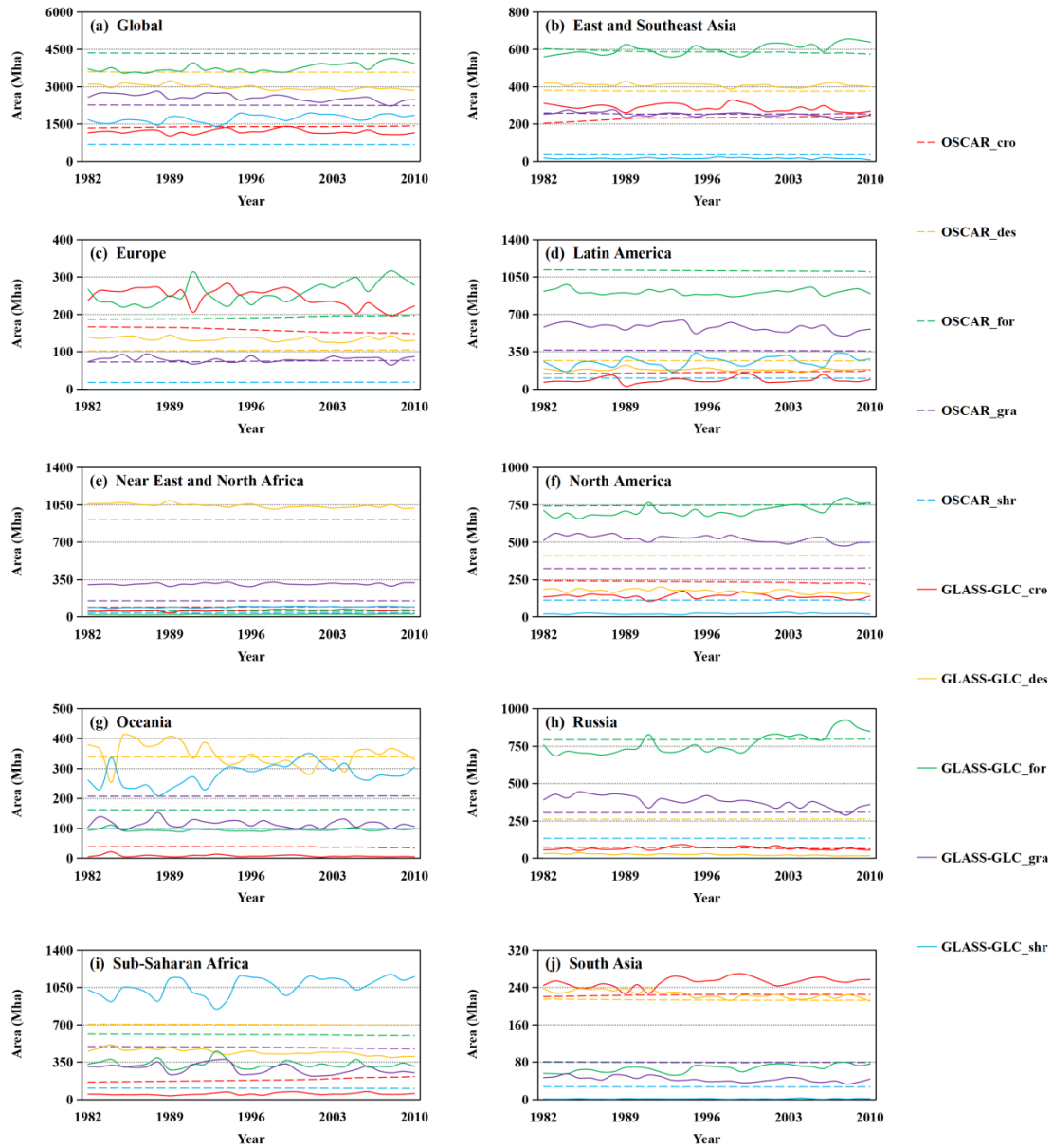
Figure S1. Areas of annual LUs (Mha) from GLASS-GLC datasets (solid line) and OSCAR inventory (dotted line) in five land-use types. The red line represents the area of cropland, the yellow line represents the area of desert, the green line represents the area of forest, the purple line represents the area of grassland and the blue line represents the area of shrubs. (a). Global, (b). East and Southeast Asia, (c). Europe, (d). Latin America, (e), Near East and North Africa, (f). North America, (g). Oceania, (h). Russia, (i). Sub-Saharan Africa, (j). South Asia.
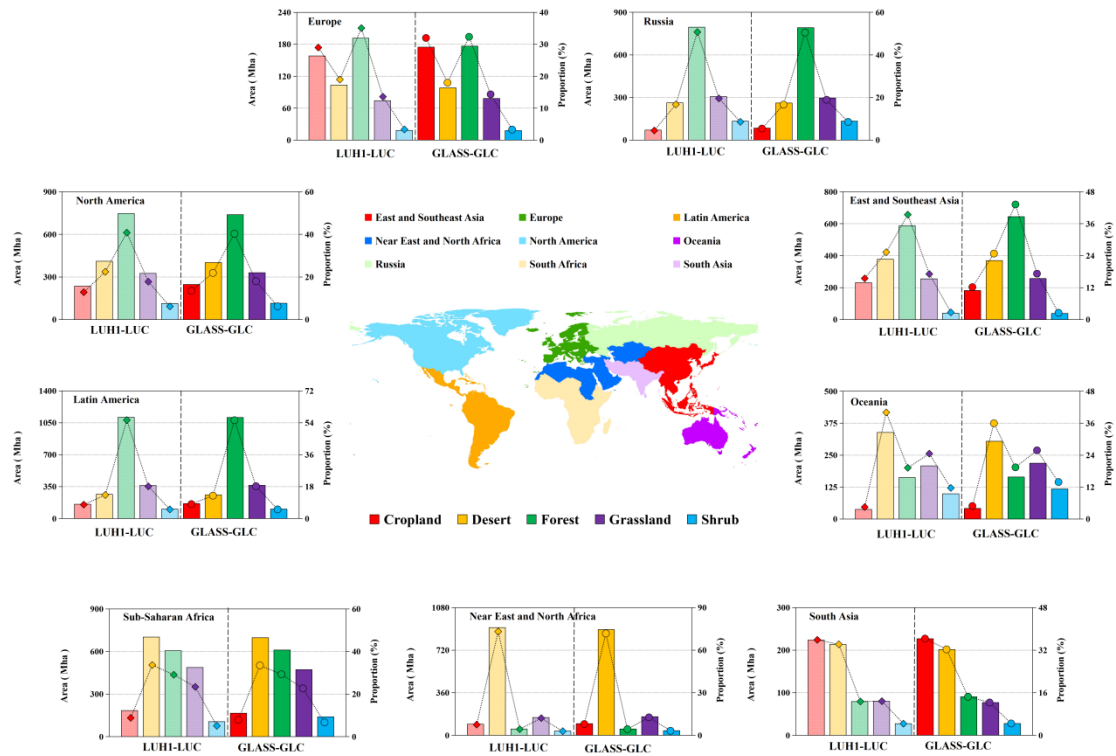
Figure S2. Area of five land use types in each of nine region and their respective percentage in the total area of nine regions. The bars in the bar chart represent the areas of five LU types in nine regions in the OSCAR LUH1-LUC (coarse resolution, scaled on the left Y-axis) and GLASS-GLC (fine resolution, scaled on the left Y-axis), namely, cropland (red), desert (yellow), forest (green), grassland (purple), and shrub (blue). Small diamonds in the bar chart represents the proportion of each land use type in the nine regions in the OSCAR dataset (scaled on the right Y-axis); small circles in the bar chart represents the proportion of each land use type in the nine regions in GLASS-GLC dataset (scaled on the right Y-axis). The nine color bars represent different regions, which can be identified in figure legend.
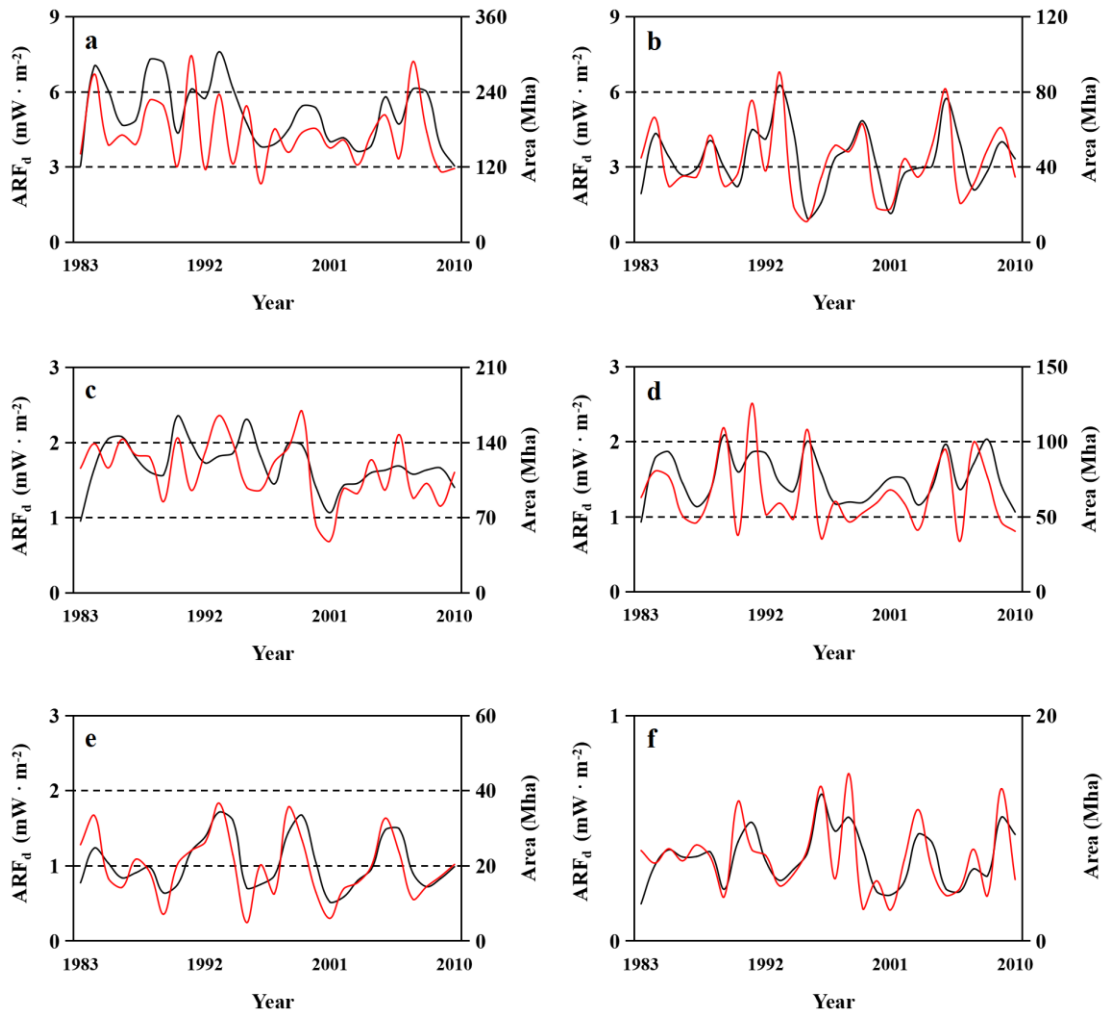
Figure S3. ARF_d in OSCAR modeled RF (solid black line) from the transition of selected LUCs in the globe. The vibration is estimated by $ARF_{di}^t = (RF^t - RF_i'^{\ t}) - (RF^{t-1} - RF_i'^{\ t-1})$, where RF^t and $RF_i'^{\ t}$ represent ARF in year t and ARF in the same year from sensitivity experiment for land conversion type i. The solid red line indicates transition area (Mha) of LU conversion types between 1982 and 2010. (a). ARF_d and transition area for grassland to forest; (b). same as Figure S3a but for shrub to forest; (c). same as Figure S3a. but for grassland to cropland; (d). same as Figure S3a but for cropland to forest; (e). same as Figure S3a but for shrub to cropland; (f). same as Figure S3a but for desert to cropland.
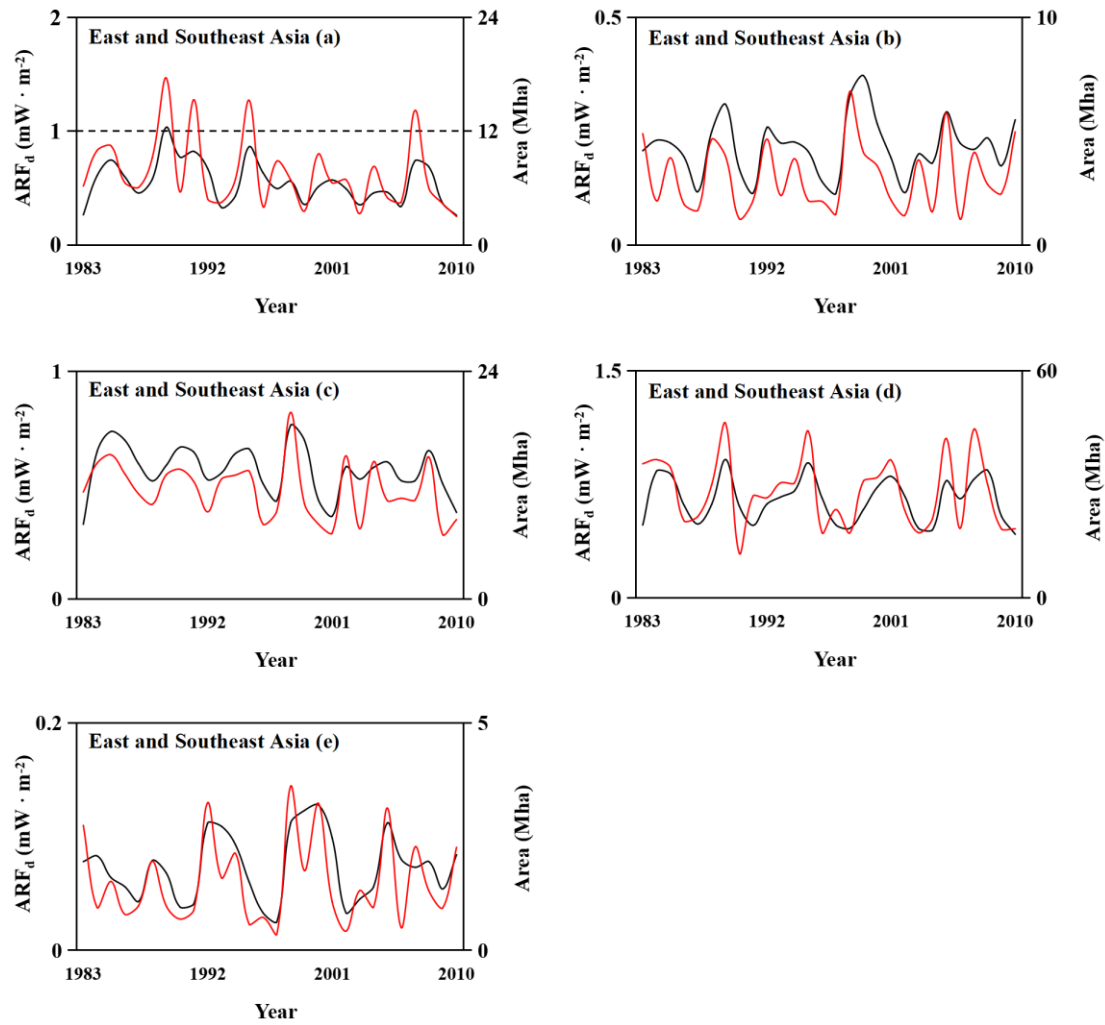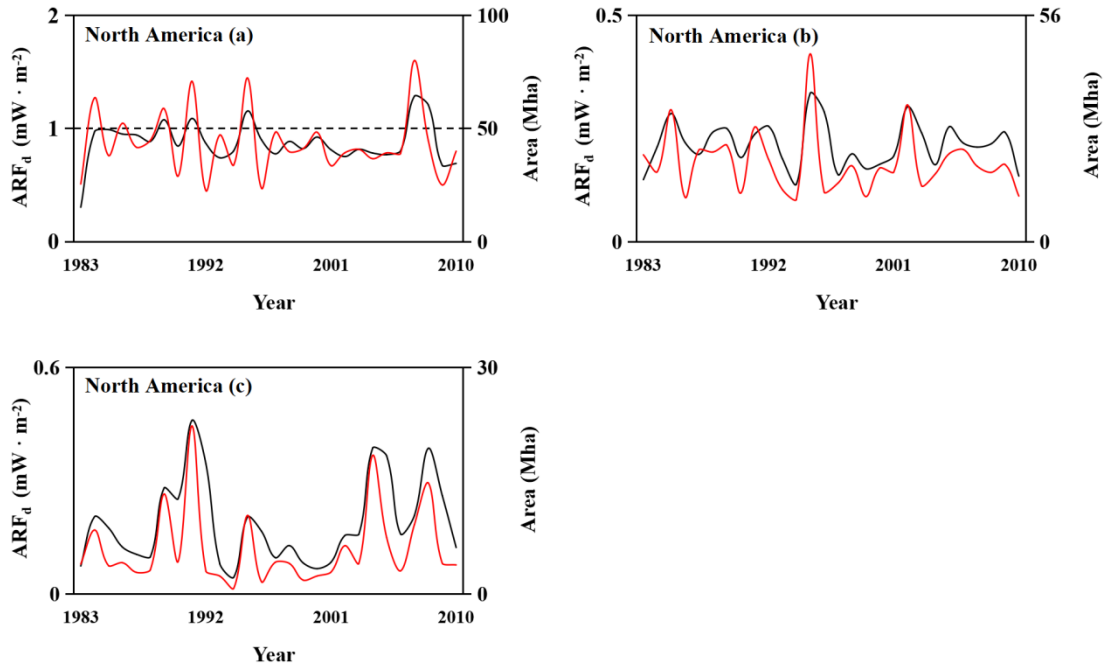
Figure S4. Same as Figure S3 but for ARF_d in OSCAR modeled RF (solid black line) from the transition of selected LUCs in East and Southeast Asia. (a). ARF_d and transition area for grassland to forest; (b). same as Figure S4a but for shrub to forest; (c). same as Figure S4a but for grassland to cropland; (d). same as Figure S4a but for cropland to forest; (e). same as Figure S4a but for shrub to cropland.
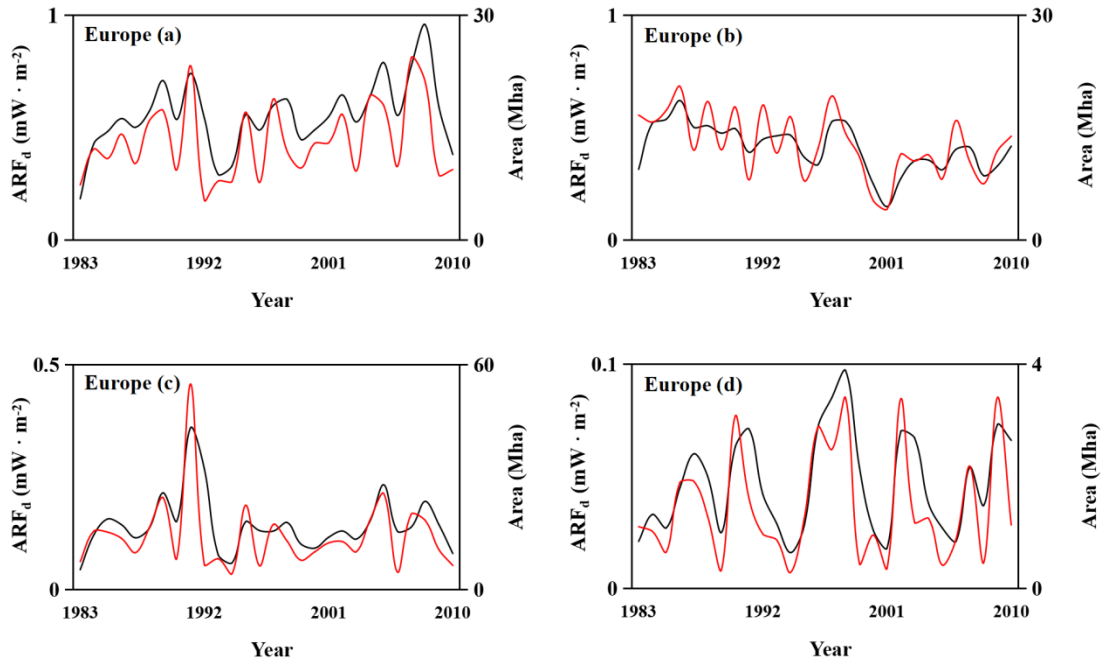
Figure S5. Same as Figure S3 but for ARF_d in OSCAR modeled RF (solid black line) from the transition of selected LUCs in Europe. (a). ARF_d and transition area for grassland to forest; (b). same as Figure S5a but for grassland to cropland; (c). same as Figure. S5a but for cropland to forest; (d). same as Figure S5a but for desert to cropland.
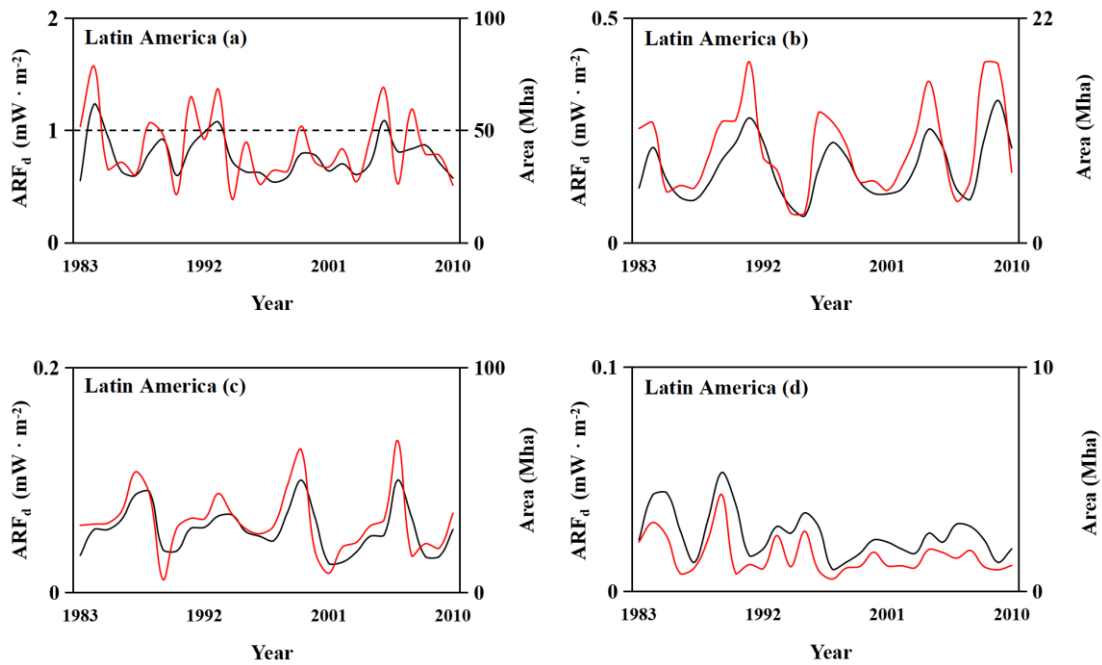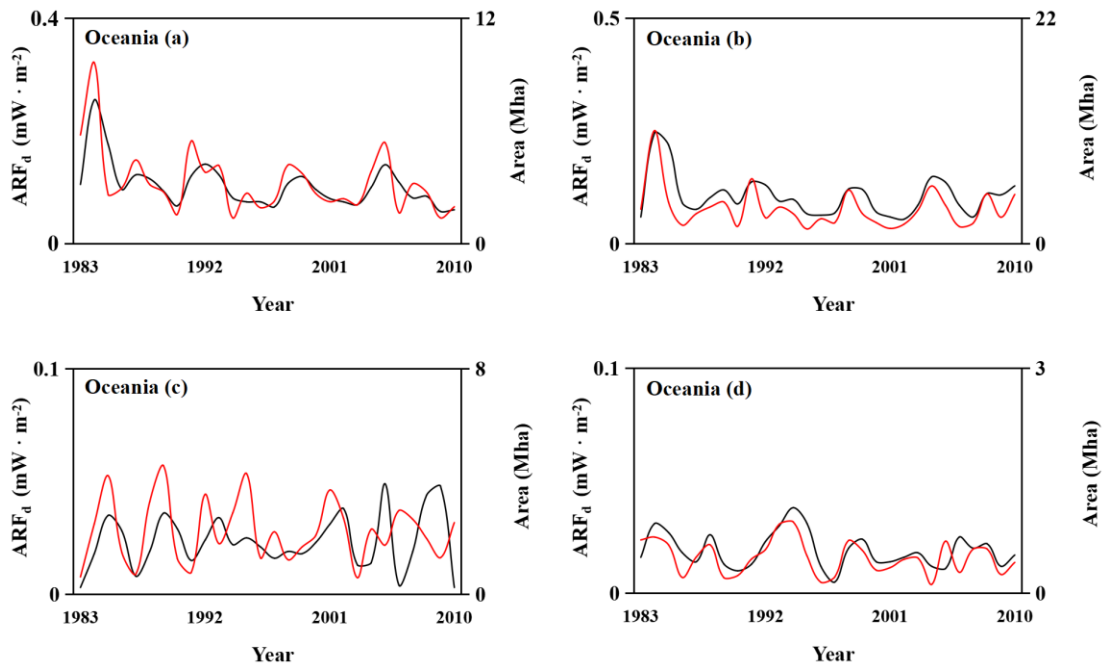

Figure S6. Same as Figure S3 but for ARF_d in OSCAR modeled RF (solid black line) from the

transition of selected LUCs in Latin America. (a). ARF_d and transition area for grass to forest; (b). same as Figure S6a but for shrub to forest; (c). same as Figure S6a but for grass to cropland; (d). same as Figure S6a but for cropland to forest.
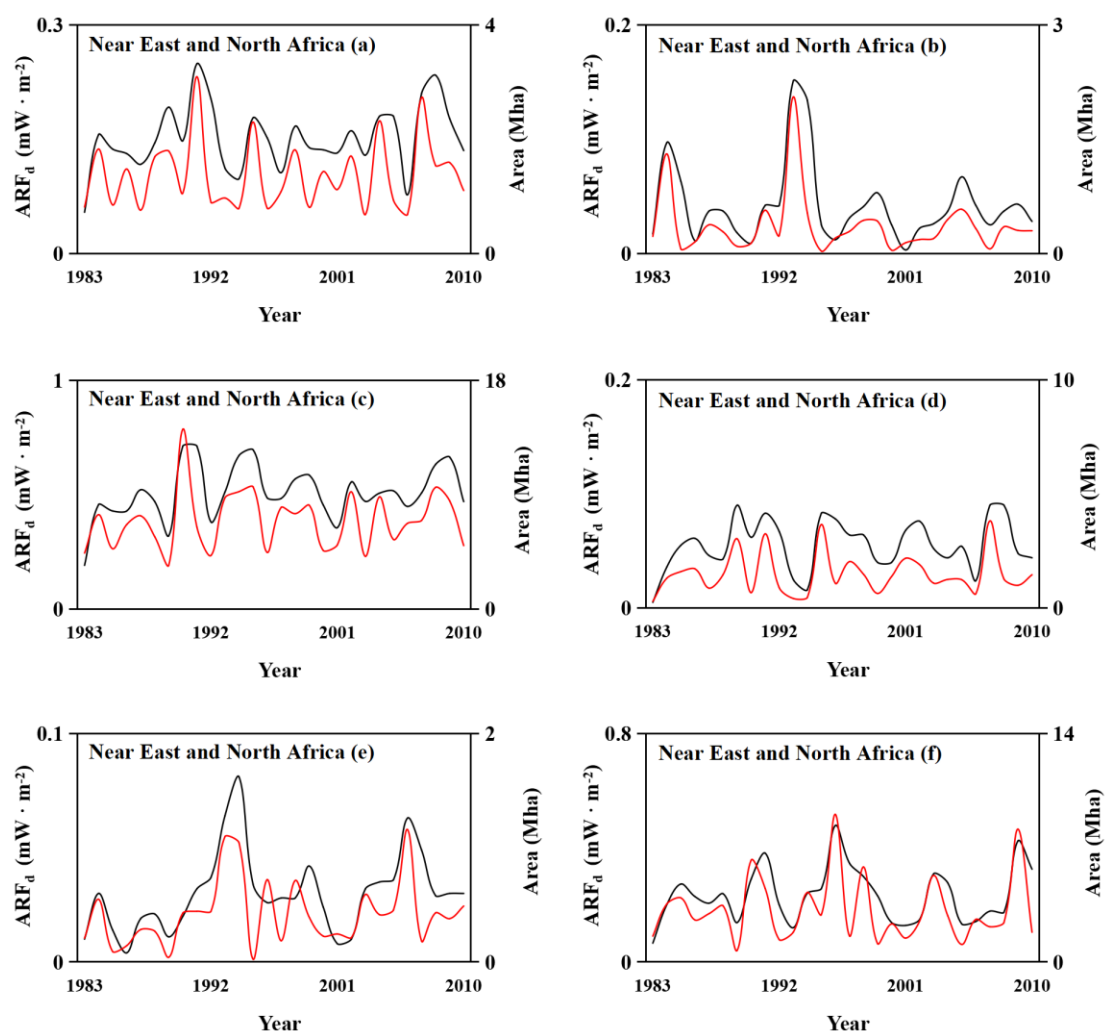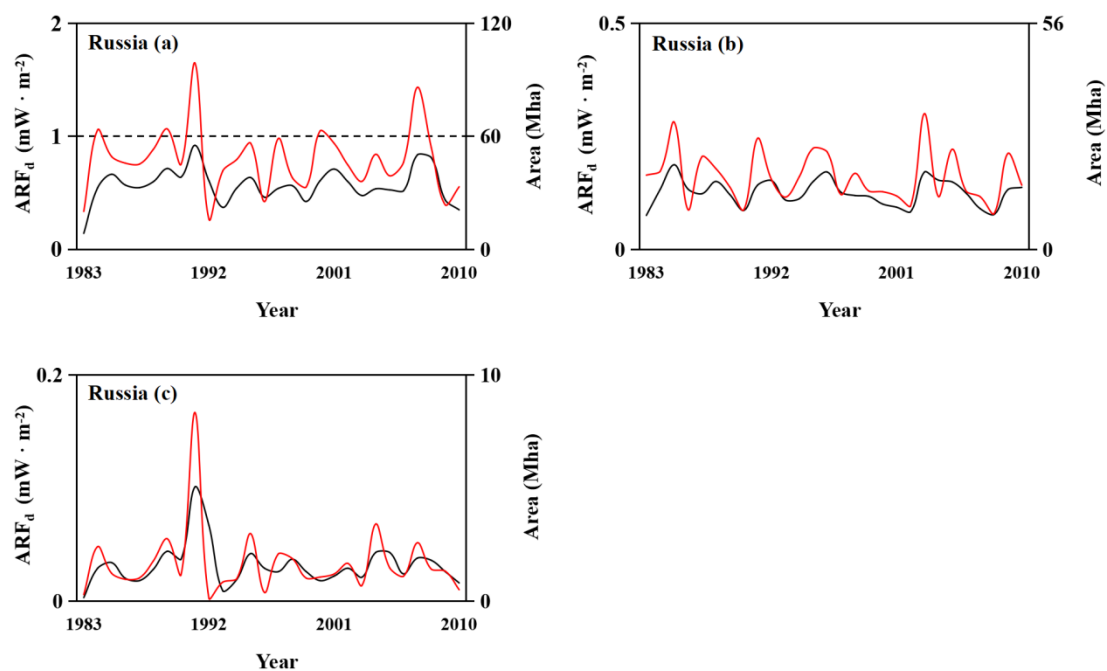

Figure S7. Same as Figure S3 but for ARF_d in OSCAR modeled RF (solid black line) from the transition of selected LUCs in ed LUCs in Near East and North Africa. (a). ARF_d and transition area for grassland to forest; (b). same as Figure S7a but for shrub to forest; (c). same as Figure S7a but for grassland to cropland; (d). same as Figure S7a but for cropland to forest; (e). same as Figure S7a but for shrub to cropland; (f). same as Figure S7a but for desert to cropland.

Figure S8. Same as Figure S3 but for ARF$_d$ in OSCAR modeled RF (solid black line) from the transition of selected LUCs in North America. (a). ARF$_d$ and transition area for grassland to forest; (b). same as Figure S8a but for cropland to grassland; (c). same as Figure S8a but for cropland to forest.
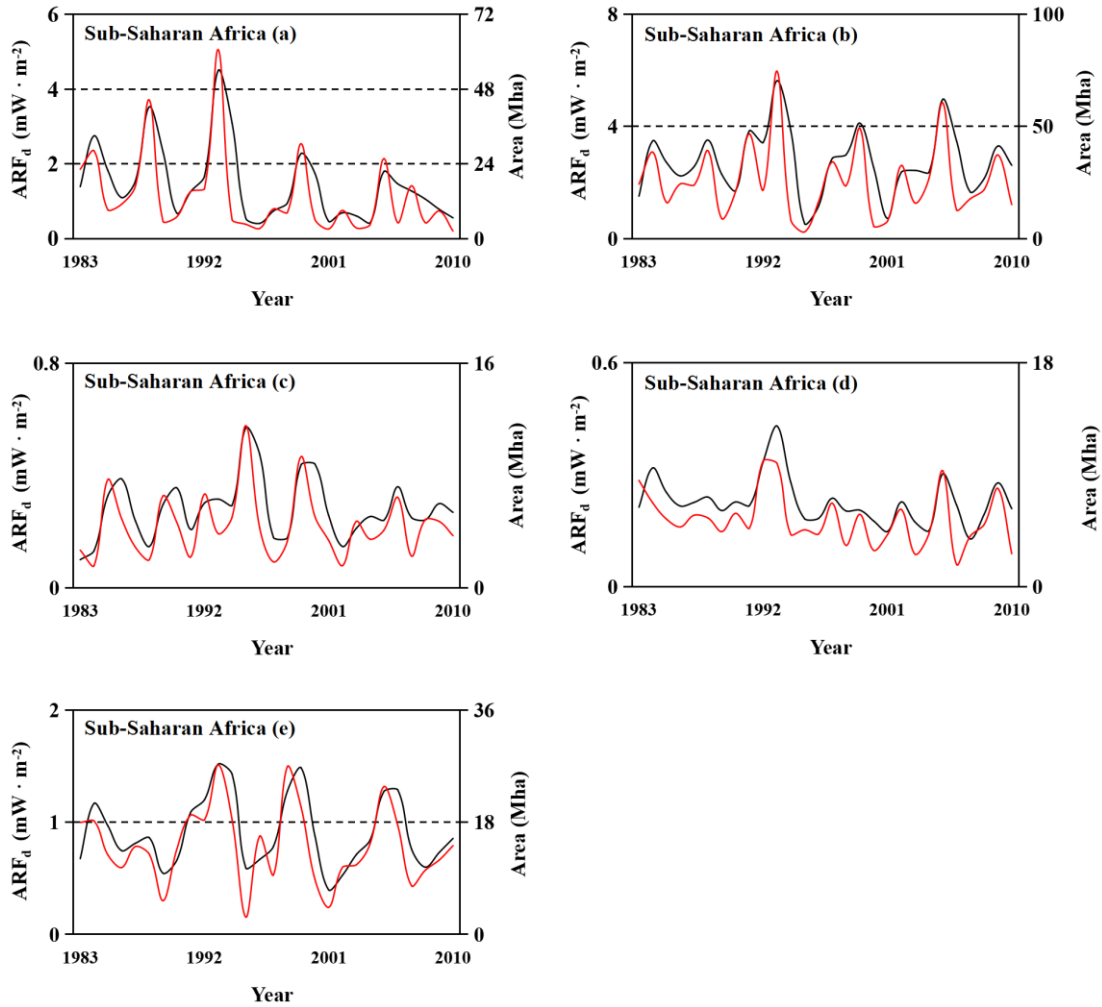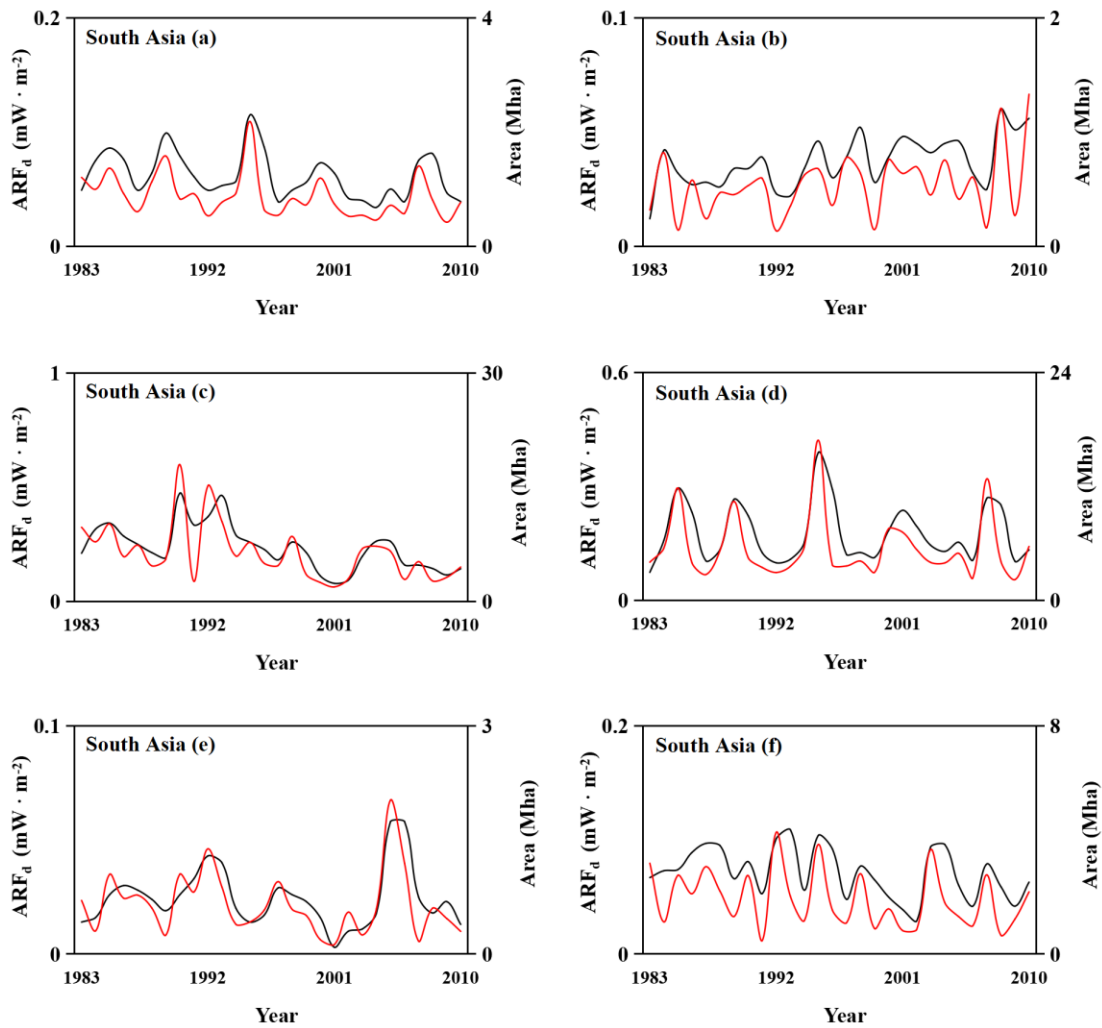

Figure S9. Same as Figure S3 but for ARF$_d$ in OSCAR modeled RF (solid black line) from the

transition of selected LUCs in Oceania. (a). ARF_d and transition area for grassland to forest; (b). same as Figure S9a but for shrub to forest; (c). same as Figure S9a but for cropland to grassland; (d). same as Figure S9a but for cropland to forest.

Figure S10. Same as Figure S3 but for ARF_d in OSCAR modeled RF (solid black line) from the transition of selected LUCs in Russia. (a). ARF_d and transition area for grassland to forest; (b). same as Figure S10a but for cropland to grassland; (c). same as Figure S10a but for cropland to forest.

Figure S11. Same as Figure S3 but for ARF_d in OSCAR modeled RF (solid black line) from the transition of selected LUCs in Sub-Saharan Africa. (a). ARF_d and transition area for grassland to forest; (b). same as Figure S11a but for shrub to forest; (c). same as Figure S11a but for grassland to cropland; (d). same as Figure S11a but for cropland to forest; (e). same as Figure S11a but for shrub to cropland.

Figure S12. Same as Figure S3 but for ARF$_d$ in OSCAR modeled RF (solid black line) from the transition of selected LUCs in South Asia. (a). ARF$_d$ and transition area for grassland to forest; (b). same as Figure S12a but for shrub to forest; (c). same as Figure S12a but for grassland to cropland; (d). same as Figure S12a but for cropland to forest; (e). same as Figure S12a but for shrub to cropland; (f). same as Figure S12a but for desert to cropland.
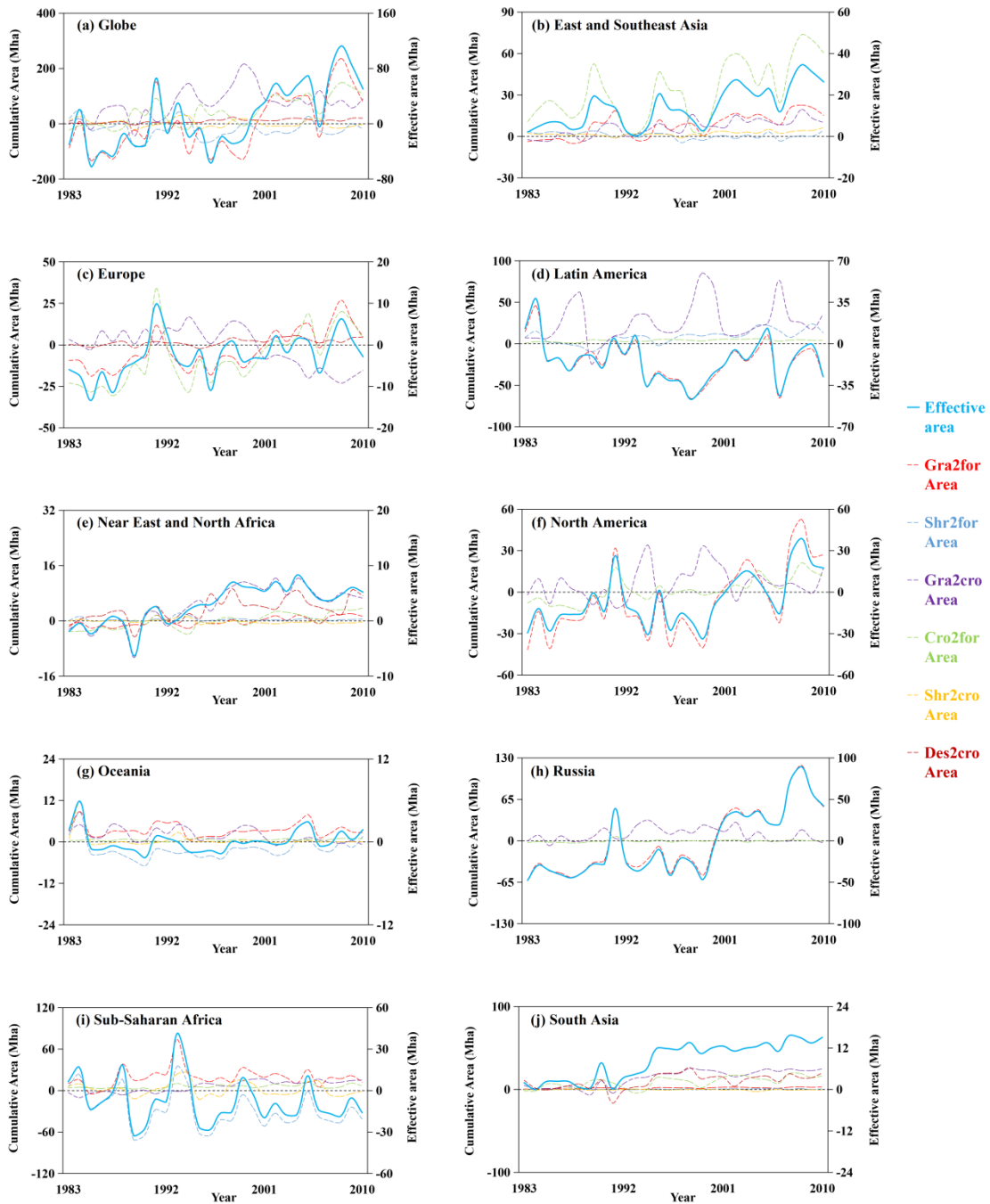
Figure S13. Effective areas in the globe and nine regions (solid blue line, scaled on the right Y-axis) and the cumulative area of the six net LU conversion types that constitute the effective area (scaled on the left Y-axis) from grassland to forest (scarlet), shrub to forest (dashed blue), grassland to cropland (purple), cropland to forest (green), shrub to cropland (yellow), and desert to cropland (solid red), respectively. (a). Effective areas in the globe and cumulative area for grassland to forest, shrub to forest, grassland to cropland, cropland to forest, shrub to cropland, and desert to cropland;

36

(b). Effective areas in East and Southeast Asia and cumulative area summed over grassland to forest, shrub to forest, grassland to cropland, cropland to forest, and shrub to cropland; (c). Effective areas in Europe and cumulative area summed over grassland to forest, grassland to cropland, cropland to forest, and desert to cropland; (d). Effective areas in Latin America and cumulative area summed over grassland to forest, shrub to forest, grassland to cropland, and cropland to forest; (e). Effective areas in Near East and North Africa and cumulative area summed over grassland to forest, shrub to forest, grassland to cropland, cropland to forest, shrub to cropland, and desert to cropland; (f). Effective areas in North America and cumulative area summed over grassland to forest, grassland to cropland, and cropland to forest; (g). Effective areas in Oceania and cumulative area summer over grassland to forest, shrub to forest, grassland to cropland, cropland to forest, and shrub to cropland; (h). Effective areas in Russia and cumulative area summed over grassland to forest, grassland to cropland, and cropland to forest; (i). Effective areas in Sub-Saharan Africa and cumulative area summed over grassland to forest, shrub to forest, grassland to cropland, cropland to forest, and shrub to cropland; (j). Effective areas in South Asia and cumulative area summed over grassland to forest, shrub to forest, grassland to cropland, cropland to forest, shrub to cropland and desert to cropland.
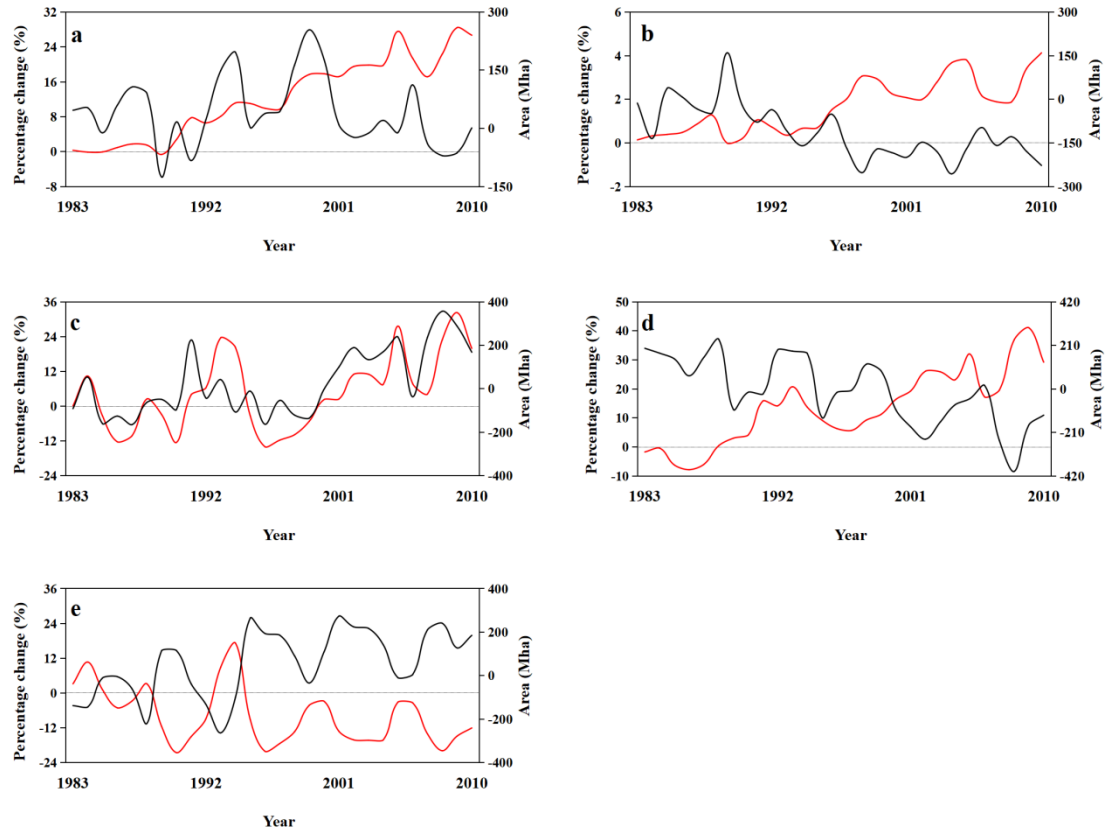
-

Figure S14. Percentage-change in OSCAR modeled RF (solid red line) from the transition of each of five LUs to the rest four LUs. The percentage change is estimated by $F_{RF} = (ARF_{S2, i} - ARF_{S2}) / ARF_{S2} \times 100\%$, where $ARF_{S2, i}$ (i=1, 2, …5) is the ARF from ith fixed LU in GLASS-GLC inventory (S2_land-use) and ARF_{S2} is the ARF from model scenario 2. The solid black line indicates accumulated transition area (Mha) of different land use types between 1982 and 2010 (scaled on the right Y-axis). (a). Percentage-change in ARF and accumulated area for cropland; (b). same as Figure. S4a but for desert; (c). same as Figure S4a but for forest; (d). same as Figure. S4a but for grassland; (e). same as Figure. S4a but for shrub land.
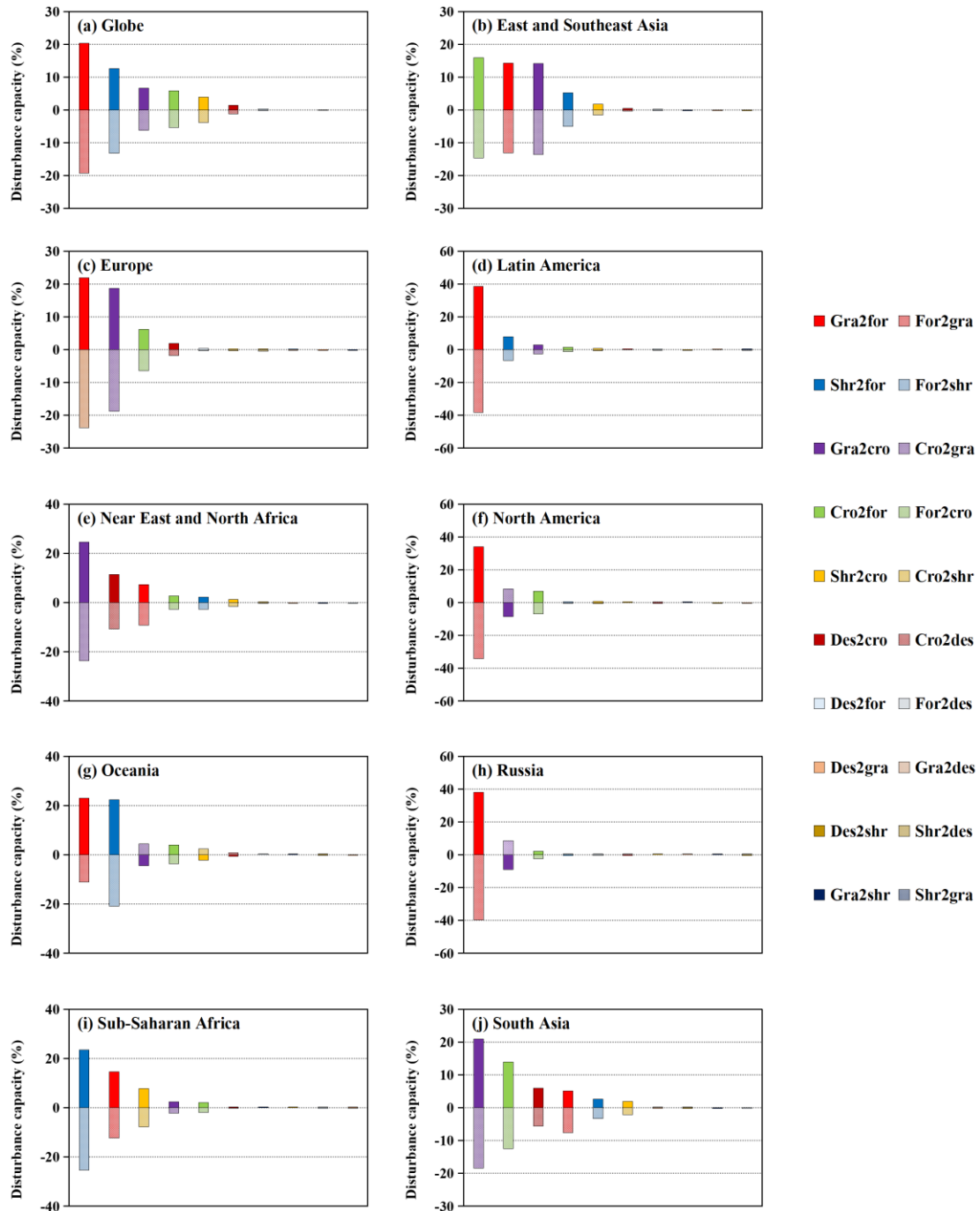
Figure S15. Histogram of disturbance capacity in the globe and nine regions, each including 20 land conversion types. The 20 types of LU transformations represented by the 20 color dwellings are shown in figure legends on the right of the figure. (a). Globe; (b). East and Southeast Asia; (c). Europe; (d). Latin America; (e). Near East and North Africa; (f). North America; (g). Oceania; (h). Russia; (i). Sub-Saharan Africa; (j). South Asia.

References

Andrews, T., Betts, R. A., Booth, B. B. B., Jones, C. D., and Jones, G. S.: Effective radiative forcing from historical land use change, Clim. Dyn., 48, 3489–3505, https://doi.org/10.1007/s00382-016-3280-7, 2017.

Betts, R. A.: Biogeophysical impacts of land use on present-day climate: near-surface temperature change and radiative forcing, Atmos. Sci. Lett., 2, 39–51, https://doi.org/10.1006/asle.2001.0023, 2001.

Bright, R. M., and Kvalevåg, M. M.: Technical Note: Evaluating a simple parameterization of radiative shortwave forcing from surface albedo change, Atmos. Chem. Phys., 13, 11169–11174, https://doi.org/10.5194/acp-13-11169-2013, 2013.

Cherubini, F., Gasser, T., Bright, R. M., Ciais, P., and Strømman, A. H.: Linearity between temperature peak and bioenergy CO_2 emission rates, Nat. Clim. Chang., 4, 983–987, https://doi.org/10.1038/nclimate2399, 2014.

Fu, B., Gasser, T., Li, B. G., Tao, S., Ciais, P., Piao, S. L., Balkanski, Y., Li, W., Yin, T. Y., Han, L. C., Li, X. Y., Han, Y. M., An, J., Peng, S. Y., and Xu, J.: Short-lived climate forcers have long-term climate impacts via the carbon-climate feedback, Nat. Clim. Chang., 10, 851–855, https://doi.org/10.1038/s41558-020-0841-x, 2020.

Gasser, T., Ciais, P., Boucher, O., Quilcaille, Y., Tortora, M., Bopp, L., and Hauglustaine, D.: The compact Earth system model OSCAR v2.2: description and first results, Geosci. Model Dev., 10, 271–319, https://doi.org/10.5194/gmd-10-271-2017, 2017.

Gasser, T., Kechiar, M., Ciais, P., Burke, E. J., Kleinen, T., Zhu, D., Huang, Y., Ekici, A., and Obersteiner, M.: Path-dependent reductions in CO_2 emission budgets caused by permafrost carbon release, Nat. Geosci., 11, 830–835, https://doi.org/10.1038/s41561-018-0227-0, 2018.

He, T., Liang, S. L., and Song, D. X.: Analysis of global land surface albedo climatology and spatial-temporal variation during 1981-2010 from multiple satellite products, J. Geophys. Res. Atmos., 119, 10281–10298, https://doi.org/10.1002/2014JD021667, 2014.

Houghton, J. T., Meira, F. L. G., Bruce, J., Lee, H., Callander, B. A., Haites, E., Harris, N., and Maskell, K.: Climate Change 1994. Radiative forcing of climate change

and an evaluation of the IPCC IS92 emission scenarios, Cambridge University Press, UK. pp 339 Available from Cambridge University Press, The Edinburgh Building Shaftesbury Road, Cambridge CB2 2RU ENGLAND.

Hurtt, G. C., Chini, L. P., Frolking, S., Betts, R. A., Feddema, J., Fischer, G., Fisk, J. P., Hibbard, K., Houghton, R. A., Janetos, A., Jones, C. D., Kindermann, G., Kinoshita, T., Goldwijk, K. K., Riahi, K., Shevliakova, E., Smith, S., Stehfest, E., Thomson, A., Thornton, P., Vuuren, D. P. V., and Wang, Y. P.: Harmonization of land-use scenarios for the period 1500-2100: 600 years of global gridded annual land-use transitions, wood harvest, and resulting secondary lands, Clim. Chang., 109, 117–161, https://doi.org/10.1007/s10584-011-0153-2, 2011.

Lenton, T. M., and Vaughan, N. E.: The radiative forcing potential of different climate geoengineering options, Atmos. Chem. Phys., 9, 5539–5561, https://doi.org/10.5194/acp-9-5539-2009, 2009.

Li, B. G., Gasser, T., Ciais, P., Piao, S. L., Tao, S., Balkanski, Y., Hauglustaine, D., Boisier, J. P., Chen, Z., Huang, M. T., Li, L. Z. X., Li, Y., Liu, H. Y., Liu, H. F., Peng, S. S., Shen, Z. H., Sun, Z. Z., Wang, R., Wang, T., Yin, G. D., Yin, Y., Zeng, H., Zeng, Z. Z., and Zhou, F.: The contribution of China's emissions to global climate forcing, Nature, 531, 357–361, https://doi.org/10.1038/nature17165, 2016.

Liu, H., Gong, P., Wang, J., Clinton, N., Bai, Y. Q., and Liang, S. L.: Annual dynamics of global land cover and itts long-term changes from 1982 to 2015, Earth Syst. Sci. Data, 12, 1217–1243, https://doi.org/10.5194/essd-12-1217-2020, 2020.

Myhre, G., and Myhre, A.: Uncertainties in Radiative Forcing due to Surface Albedo Changes Caused by Land-Use Changes, J. Climate, 16, 1511–1524, https://doi.org/10.1175/1520-0442(2003)016<1511:UIRFDT>2.0.CO;2, 2003.